Acta Crystallographica Section B
Structural Science
ISSN 0108-7681

Kaolin polytypes revisited *ab initio*

Patrick H. J. Mercier* and Yvon Le Page

Institute for Chemical Process and Environmental Technology (ICPET), National Research Council of Canada (NRC), 1200 Montreal Road, Ottawa, Ontario, Canada K1A 0R6

Correspondence e-mail: patrick.mercier@nrc-cnrc.gc.ca

Received 17 October 2007
Accepted 18 January 2008

The well known 36 distinguishable transformations between adjacent kaolin layers are split into 20 energetically distinguishable transformations (EDT) and 16 enantiomorphic transformations, hereafter denoted EDT*. For infinitesimal energy contribution of interactions between non-adjacent layers, the lowest-energy models must result from either (*a*) repeated application of an EDT or (*b*) alternate application of an EDT and its EDT*. All modeling, quantum input preparation and interpretation was performed with *Materials Toolkit*, and quantum optimizations with *VASP*. Kaolinite and dickite are the lowest-energy models at zero temperature and pressure, whereas nacrite and HP-dickite are the lowest-enthalpy models under moderate pressures based on a rough enthalpy/pressure graph built from numbers given in the supplementary tables. Minor temperature dependence of this calculated 0 K graph would explain the bulk of the current observations regarding synthesis, diagenesis and transformation of kaolin minerals. Other stackings that we list have energies so competitive that they might crystallize at ambient pressure. A homometric pair of energetically distinguishable ideal models, one of them for nacrite, is exposed. The printed experimental structure of nacrite correctly corresponds to the stable member of the pair. In our opinion, all recent literature measurements of the free energy of bulk kaolinite are too negative by ~ 15 kJ mol^{-1} for some unknown reason.

1. Introduction

The Athabasca oil sands are a very large bitumen deposit in Alberta (Canada). A significant fraction of the bitumen present in the oil sands is currently lost through processing problems arising from phyllosilicates/bitumen interactions during oil production from those sands. In view of current oil prices, the economic importance of phyllosilicates in oil sands can then hardly be overstated. The oil sands research effort in our group deals with a number of aspects specific to this oil exploitation. One of its goals is then to gain theoretical and practical insight into phyllosilicates/bitumen adhesion, with the hope of maybe finding a solution to the corresponding bitumen loss. Kaolin minerals and illites are the major phyllosilicates in those deposits, hence the present contribution on the kaolin family of minerals. At the same time, the use of kaolin minerals in ceramics, in coated paper, as a food additive, in toothpaste and in cosmetics is so economically and artistically important in a variety of applications that the topic of the present manuscript could hardly be of more general interest.

The three polytypes in kaolin-group minerals observed at ambient temperature and pressure – kaolinite, dickite and

nacrite – have the chemical composition $Al_2Si_2O_5(OH)_4$. Together with halloysite, a hydrated kaolin species for which no three-dimensional crystal-structure refinement has been performed, kaolinite, dickite and nacrite are among the most common clay minerals on the surface of the earth (Murray, 1991; kaolinite: space group $C1$, $Z = 2$; Drits & Kashaev, 1960; Zvyagin, 1960; Adams, 1983; Bish & Von Dreele, 1989; Smrčok *et al.*, 1990; Bish, 1993; Neder *et al.*, 1999; space group $P1$ – actually amounting to $C1$ – $Z = 2$; Suitch & Young, 1983; Young & Hewat, 1988; El-Sayed *et al.*, 1990; dickite: space group Cc, $Z = 2$; Newnham, 1962; Adams & Jefferson, 1976; Adams, 1979; Joswig & Drits, 1986; Bish & Johnston, 1993; Dera *et al.*, 2003; nacrite: space group Cc, $Z = 2$; Blount *et al.*, 1969; Zvyagin *et al.*, 1972; Toraya *et al.*, 1980; Zheng & Bailey, 1994). A new polytype, which occurs from dickite through a layer-shift structural phase transformation at around 2.0 GPa under hydrostatic compression, has also been observed using single-crystal X-ray diffraction (Dera *et al.*, 2003). It is designated below as HP-dickite. Those polymorphs are all based on a composite 1:1 layer comprising a sheet of edge-sharing AlO_6 octahedra stacked over a sheet of corner-linked SiO_4 tetrahedra (Giese, 1988). As the architecture of those composite layers is basically the same, kaolinite, dickite, HP-dickite and nacrite only differ in the way those layers are stacked. We wish to clarify here the issue of low-energy and thus possibly existing stackings of kaolin layers, as opposed to the complete enumeration of their geometrically distinguishable stackings. This topic was first tackled qualitatively by Newnham (1962) through the examination of the geometry of Si/Al cation–cation superposition across the inter-layer, as well as $OH\cdots O$ distances in ideal models. Instead we wish to explore here the quantitative total-energy arguments that are available nowadays through *ab initio* density-functional theory (DFT) optimization of ideal kaolin polytype models.

2. Computations

2.1. *Ab initio* modeling

The modeling and *ab initio* interface software environment *Materials Toolkit* (Le Page & Rodgers, 2005) was used to prepare input files for *ab initio* total-energy minimization calculations with *VASP* (Kresse, 1993; Kresse & Hafner, 1993, 1994). The following execution parameters were used in general: GGA PAW potentials (Kresse & Joubert, 1999); electronic convergence at 1×10^{-7} eV; convergence for forces smaller than 1×10^{-3} eV Å^{-1}; Davidson-blocked iterative optimization of the wavefunctions in combination with reciprocal-space projectors (Davidson, 1983); reciprocal space integration with a Monkhorst–Pack scheme (Monkhorst & Pack, 1976); and a Methfessel–Paxton smearing scheme of order 1 and width 0.2 eV for energy corrections (Methfessel & Paxton, 1989). Spin-polarization corrections were not used. A sufficiently large number of single-point energy-minimization iterations was completed for each simulation to ensure proper convergence of atom relaxation, calculated energy and stress. Whereas many optimizations were performed with k meshes such as $4 \times 4 \times 2$, all final calculations of total energy and residual stress were performed with a $6 \times 6 \times 6$ k mesh. The calculations required about 1 d per structure for single-layer models, 2–3 d for two-layer and three-layer models, and ~ 2 weeks for six-layer models. A Xeon cluster running serial *VASP*4.6.3 under Linux was used for most computations.

2.2. Polytype builder tool

We assembled a polytype builder tool as a new module within *Materials Toolkit* (Le Page & Rodgers, 2005). It accepts as input the description of a model for a slab in the space group $P1$, as well as instructions for stacking similar slabs. Those instructions consist of any number of typed-in lines, each one including a rotation angle and two fractional components for a translation vector parallel to the slab. The tool first interprets the slab as the content between $z = 0$ and 1 of the supplied model. The implicit perpendicular component of the slab-to-slab translation is the thickness of that slab. The rotation angle and translation on the nth line are implemented as the transformation that produces the $n + 1$ layer from the n layer considered to be referred to its standard origin and standard orientation. Each rotation must preserve at least approximately the (**a**, **b**) mesh. The sum of input layer-to-layer rotations must of course be zero or an integer number of full turns. The last input line then produces a layer corresponding to the initial one through a translation, thus defining the **c** repeat for the polytype assembled in this way. Upon exiting the tool, that polytype model in the space group $P1$ resides in the *Toolkit* structure buffer, ready for further automated manipulation such as symmetry determination or quantum optimization. In other words, the user specifies only the architecture of layer 1 and a series of p operations, the nth of which creates layer $n + 1$ from layer n. The tool then derives the rotation and translation that relates layer 1 and layer $n + 1$ and implements it, creating the complete p-layer model and its primitive cell from conceptually simple input data. The corresponding conventional crystallographic description is produced by the *Symmetry* module of *Materials Toolkit*. Input files for *VASP* optimization are prepared seamlessly with another *Toolkit* module.

3. Architecture of kaolin layers and their possible stackings

The topic of the architecture of kaolin layers and their possible stackings is fairly complex because different description schemes were used (Newnham, 1962; Zvyagin, 1962; Bailey, 1963; Dornberger-Schiff & Durovič, 1975*a*,*b*; Durovič *et al.*, 1981), because many printed structure illustrations are poor by current standards, and because it is not straightforward to grasp all 36 possible stackings at once. Fortunately, this complexity can be broken down into two steps by considering first the simpler case of lizardite layers $Mg_3Si_2O_5(OH)_4$ with $3m$ point-group symmetry comprising trioctahedral sheets, and thus only eight possible stackings resulting from all combinations of four translations with two rotations. The

Table 1
(*a*) Lizardite 1*T* at 8 K, including hydrogen positions, space group *P*31*m* (Gregorkiewitz *et al.*, 1996); (*b*) idealized model for lizardite 1*T* in space group *P*1; (*c*) idealized model kaolin K1*a* (zero rotation, zero translation) in space group *P*1 derived from (*b*).

(*a*) Lizardite 1*T*†				
Si	2(*b*)	1/3	2/3	0.070
Mg	3(*c*)	0.324	0	0.447
O1	2(*b*)	1/3	2/3	0.292
O2	3(*c*)	0.507	0	−0.014
O3	3(*c*)	0.665	0	0.587
O4	1(*a*)	0	0	0.291
H3	3(*c*)	0.646	0	0.715
H4	3(*c*)	0.046	0.046	0.172
(*b*) Ideal lizardite 1*T* in *P*31*m*				
Si	2(*b*)	1/3	2/3	0.070
Mg	3(*c*)	1/3	0	0.447
O1	2(*b*)	1/3	2/3	0.292
O2	3(*c*)	1/2	0	−0.014
O3	3(*c*)	2/3	0	0.587
O4	1(*a*)	0	0	0.291
H3	3(*c*)	2/3	0	0.715
H4	1(*a*)	0	0	0.172
(*c*) Ideal kaolin model K1*a* in *P*1‡				
Si1	1(*a*)	0.333333333	0.666666667	0.137931035
Si2	1(*a*)	0.666666667	0.333333333	0.137931035
Al3	1(*a*)	0.333333333	0.000000000	0.515133834
Al4	1(*a*)	0.000000000	0.333333333	0.515133834
O5	1(*a*)	0.333333333	0.666666667	0.360050455
O6	1(*a*)	0.666666667	0.333333333	0.360050455
O7	1(*a*)	0.500000000	0.000000000	0.053885848
O8	1(*a*)	0.000000000	0.500000000	0.053885848
O9	1(*a*)	0.500000000	0.500000000	0.053885848
O10	1(*a*)	0.666666667	0.000000000	0.655209145
O11	1(*a*)	0.000000000	0.666666667	0.655209145
O12	1(*a*)	0.333333333	0.333333333	0.655209145
O13	1(*a*)	0.000000000	0.000000000	0.359049917
H14	1(*a*)	0.666666667	0.000000000	0.783278000
H15	1(*a*)	0.000000000	0.666666667	0.783278000
H16	1(*a*)	0.333333333	0.333333333	0.783278000
H17	1(*a*)	0.000000000	0.000000000	0.239985904

The origin in *x* and *y*, common to all the reference systems above except Zvyagin, is through the centre of the hexagon of silicate tetrahedra. Kaolin layers are polar along *z*. The origin of the *z* coordinates is often selected at the basal O atoms of the Si tetrahedra. † Note that H4 is disordered with occupancy 1/3. Formula: $Mg_3Si_2O_5(OH)_4$, $Z = 1$, space group *P*31*m*, $a = 53267$, $c = 72539$ Å. ‡ Derived from Table 1(*b*). Formula: $Al_2Si_2O_5(OH)_4$, $Z = 1$, space group *P*1, $a = 5.3267$, $b = 5.3267$, $c = 7.2539$ Å, $\alpha = 90$, $\beta = 90$, $\gamma = 120°$.

stackings of kaolin layers comprising dioctahedral sheets then logically follow as straightforward subdivisions among those of lizardite, resulting in all combinations of six rotations and six translations. Readers familiar with the topic of kaolin-layer stackings can accordingly skip the following paragraphs up to §3.4.1.

3.1. Lizardite layers

Gregorkiewitz *et al.* (1996) report the lizardite 1*T* structure including its H atoms. We list their structure results in Table 1(*a*), together with an ideal model in Table 1(*b*), where *x* and *y* fractional coordinates are rounded to integer multiples of sixths. Its $Mg_3Si_2O_5(OH)_4$ electrically neutral composite layer can be thought of as a $Mg(OH)_2$ brucite layer (Fig. 1*a*) sharing apical hydroxyls with a $Si_2O_3(OH)_2$ layer (Fig. 1*b*). An O atom remains where hydroxyls are shared, resulting in composite layers (Fig. 1*c*) of $Mg_3Si_2O_5(OH)_4$ with the point group 31*m* oriented by its short translations. As there is only one way to perform this operation, there is only one architecture for the lizardite layer. Valence sums in Pauling's sense (Pauling, 1960) are perfectly obeyed within the layers. Mg^{2+} ions in octahedra share 1/3 valence unit (v.u.) with each oxygen neighbour, whereas Si^{4+} in tetrahedra shares 1 v.u. with each oxygen neighbour. Basal plane O atoms have two Si neighbours, thus summing up to −2 v.u. The apical O atoms of the tetrahedra are shared between one Si and three Mg atoms. An O^{2-} ion at those locations then balances the formal valences of the bonds reaching it. The unshared intra-layer oxygen in the mid-layer as well as the top inter-layer O atoms all have three Mg neighbours. An $(OH)^-$ group at those locations then satisfies Pauling's valence sums. The lizardite layer can then be seen as a neutral inorganic biperiodic polymer.

3.2. Distinguishable stackings of two lizardite layers

We are not trying here to establish a list of all the lizardite polytypes, which has already been discussed elsewhere (Bailey, 1988; Bailey & Banfield, 1995; Banfield *et al.*, 1995; Banfield & Bailey, 1996), but just the distinguishable ways to stack two lizardite layers, the first one of which is referred to its standard origin in standard orientation defined by the structure description reported in Gregorkiewitz *et al.* (1996). Lizardite exists as a triperiodic crystalline material because the top brucite OH anions of its polymeric 1:1 layers establish weak hydrogen bonds with the basal-plane O atoms shared between two Si atoms as seen by examining the stacking of lizardite 1*T* (Fig. 1*d*). Different stackings of lizardite layers (symmetry 31*m*) are accordingly possible and distinguishable for the following reasons:

(i) Translations (2**a** + **b**)/3 and (**a** + 2**b**)/3 repeat the brucite sheet (Fig. 2*a)* in the lizardite reference system (Fig. 2*b*). Under such displacement of the top lizardite layer, the same set of hydrogen bonds is then formed between the silicate and brucite sheets of adjacent layers, whereas silicate networks superpose differently.

(ii) Translations of the top layer by **a**/3, **b**/3 or 2(**a** + **b**)/3 (but not −**a**/3 *etc.*) shift the centre of the silicate rings of the top layer from the vertical through the centre of an anion triangle of the brucite sheet pointing along −**a** to the vertical of the centre of a triangular face of Mg octahedra pointing along +**a**. As the silicate sheet has approximate sixfold symmetry through the centre of the silicate rings, sets of hydrogen bonds analogous to those in (i) above (Fig. 2*c*) can then form, but the layer stacking itself is different.

(iii) A rotation by $k\pi/3$ about the *z* axis of the top lizardite layer approximately or exactly reproduces the silicate sheet of the top layer with quasi-sixfold symmetry (Fig. 2*d*). If *k* is even, the same top layer with threefold symmetry is reproduced in the transformation. If *k* is odd, the rotation produces a different orientation of its brucite sheet without altering the hydrogen-bond scheme with the bottom lizardite layer.

Translations **a**/3, **b**/3 or 2(**a** + **b**)/3 are related by the threefold symmetry axis through the origin. A rotation axis is a first-

kind operation transforming an object into a superposable object. Although distinguishable from the 1*T* stacking, the stackings they generate are not distinguishable among themselves. We then need to consider only one of them, say **a**/3. Translations (2**a** + **b**)/3 and (**a** + 2**b**)/3 are mirror-related. Symmetry planes are second-kind operations transforming a general object into a non-superposable enantiomorphic object. The stackings they produce are accordingly distinguishable from one another. Rotations by zero, $2\pi/3$ and $4\pi/3$ are also symmetry-related and produce identical objects. In the same way, rotations by $\pi/3$, π and $5\pi/3$ are also symmetry-related to any one of them, say a π rotation. The distinguishable stackings of two lizardite layers can then be tabulated as the combination of a rotation and a translation. For example, the 4 × 2 table would list horizontally the two possible rotations 0 and π about *z*, and vertically the four possible translation vectors 0, (2**a** + **b**)/3, (**a** + 2**b**)/3 and **a**/3, whose combinations each give rise to different superpositions for the two layers. Eight distinguishable stackings of two lizardite layers then result, the stackings in the third row [translation (**a** + 2**b**)/3] being the enantiomorphs of those directly above in the second row and produced by translation (2**a** + **b**)/3.

3.3. Architecture of kaolin layers

The architecture of the kaolin layer derives from that of lizardite by replacing the three Mg^{2+} ions within the mesh by two Al^{3+} ions and a vacancy □. A model in the space group *P*1 of the ideal kaolin structure equivalent to the ideal lizardite 1*T* structure of Table 1(*b*) resulting from this replacement is reported in Table 1(*c*). This substitution destroys the threefold symmetry of lizardite and has been performed by replacing the Mg^{2+} atom at 2/3, 2/3, *z* along [110] in the lizardite mesh by a vacancy (Fig. 3). The modification has two effects:

(i) the point-group symmetry is reduced from 31*m* to *m*;

(ii) the perfect Pauling valence sums (Pauling, 1960) are disrupted at the six oxygen sites octahedrally coordinating with Al^{3+}.

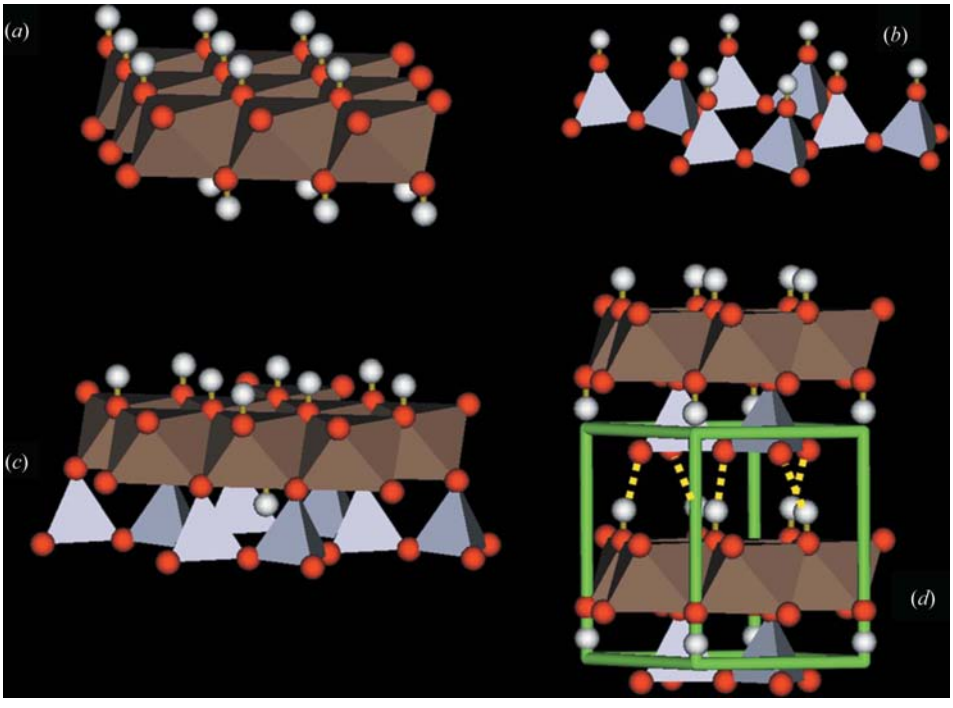

Figure 1
Assemblage of a lizardite layer. (*a*) Brucite layer; (*b*) silicate $Si_2O_3(OH)_2$; (*c*) brucite layer on the silicate layer: shared OH groups become O atoms; (*d*) hydrogen-bond network.

3.4. Distinguishable stackings of two kaolin layers

In the substitution of Mg_3^{2+} by $Al_2^{3+}\square$, the preserved mirror passes through the now vacant octahedral site at [2/3, 2/3, *z*] in the first kaolin layer (Fig. 3). Upon stacking a second layer, the distinguishable rotations that preserve the hydrogen-bonding scheme are then $k\pi/3$, k = 0–5, due to the loss in the kaolin layer of the threefold axis present in the lizardite layer. Owing to the fact that the anion network of the kaolin layer is unchanged with respect to that of the lizardite layer, vectors **0**, (2**a** + **b**)/3 and (**a** + 2**b**)/3 are still distinguishable translations that preserve the hydrogen-bonding scheme upon stacking a second kaolin layer. Vectors related to them by threefold symmetry like (−**a** + **b**)/3, −(2**a** + **b**)/3 and (**a** − **b**)/3 are equivalent to the above selections through translations of the net of the kaolin layer, and are therefore indistinguishable from them. Similar to lizardite, translations by vectors **a**/3, **b**/3 and 2(**a** + **b**)/3 also form analogous sets of hydrogen bonds, but at alternate oxygen positions around the silicate rings. It then appears that there are (6 rotations × 6 translations) = 36 distinguishable ways to stack the second layer of kaolin on top of the first one, corresponding to the 36 cells in Table 2(*a*). This result was first established by Newnham (1962), but 45 years later we felt it worthwhile to guide the reader step-by-step through this different, better-illustrated and hopefully easier-to-follow route.

3.4.1. Energetically distinguishable transformations. Owing to the mirror symmetry of the isolated ideal kaolin layer, rotations by $4\pi/3$ and $5\pi/3$ lead to enantiomorphic stackings that are mirror-related to those obtained respectively through rotations by $2\pi/3$ and $\pi/3$, and therefore energetically indistinguishable because all interatomic distances and angles are the same. In addition, translations (2**a** + **b**)/3

and (**a** + 2**b**)/3, as well as **a**/3 and **b**/3, are related by the surviving mirror through the vacancy. Their combinations with respective rotations that add up to $2k\pi$ produce energetically indistinguishable mirror-related objects. The 36 geometrically distinguishable layer transformations then split into 20 energetically distinguishable transformations (EDT) and 16 transformations that are mirror-related to an EDT and that we denote EDT*. The EDTs are listed as symbols K1*a*–K20*a* in Table 2(*a*), whereas the EDT* ones carry the symbol of the corresponding EDT appended with an asterisk.

3.4.2. Low-energy structure model generation. The above split of transformations between EDT and EDT* allows us to build potentially low-energy kaolin polytypes. Interactions between non-adjacent layers are expected to be negligible because kaolin layers are neutral inorganic biperiodic polymers. According to this concept, and provided that the stacking energies associated with the various EDTs would differ by more than those associated with non-adjacent layer interactions, the lowest-energy kaolin polytypes are then among those obtained either (*a*) by repeated application of a same EDT or (*b*) by successive application of an EDT and its EDT* where the EDT* exists. The tiny energy correction to adjacent layer interactions brought about by non-adjacent layer interactions decides which of those two models (*a*) or (*b*) will have truly the lowest energy under given crystallization conditions. At any rate, it will be one of those two models. There are 20 polytype models which are thus obtained by repeated stacking of the 20 EDTs in Table 2(*a*), whereas 16 more corresponding to the succession EDT:EDT* are listed in Table 2(*b*). Full descriptions with space group, cell data and atomic content for all those ideal models are listed in depos-

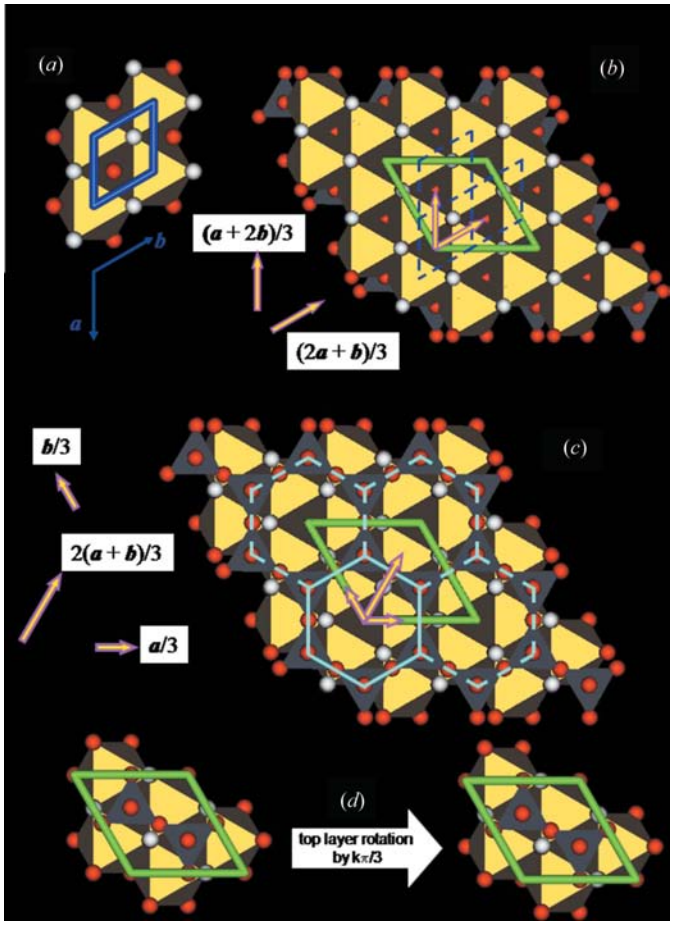

Figure 2
Lizardite vectors (**a** + 2**b**)/3 and (2**a** + **b**)/3 shown in (*b*) with a green mesh are repeats for the brucite layers shown in (*a*) with a blue mesh. (*c*) Translations by **a**/3 alter the cation superpositions, but not the OH···O network. (*d*) Rotation by $k\pi/3$ about the *z* axis of the top lizardite layer approximately or exactly reproduces the silicate sheet of the top layer with quasi-sixfold symmetry.

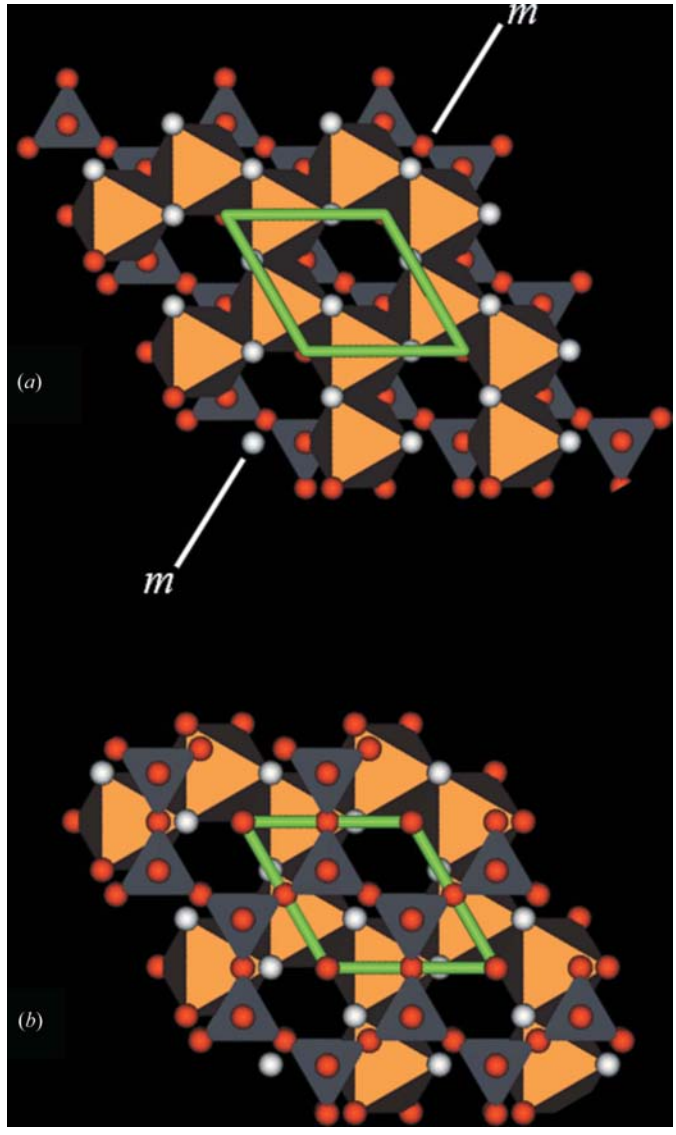

Figure 3
Kaolin layer derived from the lizardite layer. Three Mg^{2+} ions from the brucite layer in Fig. 1(*a*) are now replaced by two Al^{3+} ions in Fig. 3(*a*) with no change to the anion distribution. The resulting symmetry of the kaolin layer is accordingly *m* rather than 31*m*. The silicate sheet from Fig. 2(*b*), the silicate/Al-brucite stacking from Fig. 2(*c*) and hydrogen-bond network from Fig. 2(*d*) are unchanged.

Table 2
Low-energy stackings of two kaolin layers.

Note: 1 meV per kaolin f.u. $\simeq$ 0.0955 kJ mol^{-1}.

	Rotation					
	0	$\pi/3$	$2\pi/3$	π	$4\pi/3$	$5\pi/3$
(*a*) Repeated operations [*Kx*]						
Translation: 0						
Model No.	[K1]	[K2*a*]	[K3*a*]	[K4]	[K3*a*]*	[K2*a*]*
Space group	*Cm*	$P6_1$	$P3_1$	$Cmc2_1$	$P3_2$	$P6_5$
Free energy difference (meV per f.u.)	69	18	119	45	–	–
Volume difference (Å^3)	0.614	0.925	−1.081	0.459	–	–
Translation: $(2\mathbf{a}+\mathbf{b})/3$						
Model No.	[K5*a*]	[K6*a*]	[K7*a*]	[K8*a*]	[K10*a*]*	[K9*a*]*
Space group	*P*1	$P6_1$	$P3_1$	$P2_1$	$P3_2$	$P6_5$
Free energy difference (meV per f.u.)	137	76	117	50	–	–
Volume difference (Å^3)	−2.863	0.433	−2.879	0.236	–	–
Translation: $(\mathbf{a}+2\mathbf{b})/3$						
Model No.	[K5*a*]*	[K9*a*]	[K10*a*]	[K8*a*]*	[K7*a*]*	[K6*a*]*
Space group	–	$P6_1$	$P3_1$	–	$P3_2$	$P6_5$
Free energy difference (meV per f.u.)	–	35	105	–	–	–
Volume difference (Å^3)	–	0.439	0.297	–	–	–
Translation: $\mathbf{a}/3$						
Model No.	[K11*a*]	[K12*a*]	[K13*a*]	[K14*a*]	[K16*a*]*	[K15*a*]*
Space group	*P*1	$P6_1$	$P3_1$	$P2_1$	$P3_2$	$P6_5$
Free energy difference (meV per f.u.)	0	41	12	46	–	–
Volume difference (Å^3)	0.000	0.658	−0.085	−0.019	–	–
Translation: $\mathbf{b}/3$						
Model No.	[K11*a*]*	[K15*a*]	[K16*a*]	[K14*a*]*	[K13*a*]*	[K12*a*]*
Space group	*P*1	$P6_1$	$P3_1$	$P2_1$	$P3_2$	$P6_5$
Free energy difference (meV per f.u.)	–	53	9	–	–	–
Volume difference (Å^3)	–	0.606	0.087	–	–	–
Translation: $2(\mathbf{a}+\mathbf{b})/3$						
Model No.	[K17]	[K18*a*]	[K19*a*]	[K20]	[K19*a*]*	[K18*a*]*
Space group	*Cm*	$P6_1$	$P3_1$	*Cmc*21	$P3_2$	$P6_5$
Free energy difference (meV per f.u.)	72	183	107	131	–	–
Volume difference (Å^3)	−1.450	−1.387	−1.468	−0.972	–	–
(*b*) Succession of operations [*Kx*] and then [*Kx*]*, the enantiomorph of [*Kx*]						
Translation: 0						
Model No.	–	[K2*b*]	[K3*b*]	–	[K3*b*]* = [K3*b*]	[K2*b*]* = [K2*b*]
Space group	–	*Cc*	*Cc*	–	*Cc*	*Cc*
Free energy difference (meV per f.u.)	–	29	106	–	–	–
Volume difference (Å^3)	–	0.438	−0.860	–	–	–
Translation: $(2\mathbf{a}+\mathbf{b})/3$						
Model No.	[K5*b*]	[K6*b*]	[K7*b*]	[K8*b*]* = [K8*b*]	[K10*b*]* = [K10*b*]	[K9*b*]* = [K9*b*]
Space group	*Cc*	*Cc*	*Cc*	*Cc*	*Cc*	*Cc*
Free energy difference (meV per f.u.)	135	78	112	51	–	–
Volume difference (Å^3)	−0.796	−0.061	−2.843	0.250	–	–
Translation: $(\mathbf{a}+2\mathbf{b})/3$						
Model No.	[K5*b*]*	[K9*b*]	[K10*b*]	[K8*b*]* = [K8*b*]	[K7*b*]* = [K7*b*]	[K6*b*]* = [K6*b*]
Space group	*Cc*	*Cc*	*Cc*	*Cc*	*Cc*	*Cc*
Free energy difference (meV per f.u.)	–	59	132	–	–	–
Volume difference (Å^3)	–	−2.179	−0.826	–	–	–
Translation: $\mathbf{a}/3$						
Model No.	[K11*b*]	[K12*b*]	[K13*b*]	[K14*b*]* = [K14*b*]	[K16*b*]* = [K16*b*]	[K15*b*]* = [K15*b*]
Space group	*Cc*	*Cc*	*Cc*	*Cc*	*Cc*	*Cc*
Free energy difference (meV per f.u.)	14	32	8	24	–	–
Volume difference (Å^3)	0.189	0.367	0.046	1.016	–	–
Translation: $\mathbf{b}/3$						
Model No.	[K11*b*]*	[K15*b*]	[K16*b*]	[K14*b*]* = [K14*b*]	[K13*b*]* = [K13*b*]	[K12*b*]* = [K12*b*]
Space group	*Cc*	*Cc*	*Cc*	*Cc*	*Cc*	*Cc*
Free energy difference (meV per f.u.)	–	32	2	–	–	–
Volume difference (Å^3)	–	0.321	0.208	–	–	–
Translation: $2(\mathbf{a}+\mathbf{b})/3$						
Model No.	–	[K18*b*]	[K19*b*]	–	[K19*b*]* = [K19*b*]	[K18*b*]* = [K18*b*]
Space group	–	*Cc*	*Cc*	–	*Cc*	*Cc*
Free energy difference (meV per f.u.)	–	182	112	–	–	–
Volume difference (Å^3)	–	−1.350	−1.706	–	–	–

ited Table S1 in easy-to-read *Materials Toolkit* cut-and-paste ASCII format. We did not edit them in order to avoid transcription errors.

3.4.3. Optimization of models. The above ideal models were optimized as described in §2 above. The resulting optimized structures are also included in Table S1. The corresponding 72 CIF files for ideal and optimized models are available as supplementary material. The key results of the calculated free-energy difference with kaolinite (model K11*a*) and calculated cell-volume difference with kaolinite are also collated in Tables 2(*a*) and (*b*) for easy consulting.

4. Results and discussion

4.1. Analysis of *ab initio* results

4.1.1. Known kaolin minerals. All four currently known crystal forms of kaolin minerals are among the list of 36 models we generated. Kaolinite, dickite, nacrite and high-pressure dickite are, respectively, models K11*a*, K16*b*, K9*b* and K7*b* in Tables 2(*a*) and (*b*). This fact is in support of the energy-based reasoning in §3.4.2 above. It should be noted that all our starting models are ideal models derived from *x* and *y* atom coordinates in lizardite being rounded to fractions. However, blindly optimized models for the four known crystal forms display the cell and polyhedral distortions observed experimentally. As is well known, owing to imperfections in numerical DFT *ab initio* potentials used for the various atoms, the accuracy of DFT-calculated values for cell edges and angles does not yet match that obtainable experimentally by single-crystal or powder methods. However, the accuracy of DFT-calculated fractional coordinates for atoms matches that of most X-ray diffraction studies except the very best single-crystal studies (Mercier *et al.*, 2005). This is what we observe here, with approximate but very recognizable cell data, whereas the reproduction of experimental polyhedral rotations and distortions is amazing considering that all models were assembled from an idealized trigonal model where all *x* and *y* atom coordinates were taken as integer multiples of sixths. We are confident that the accuracy of our optimized fractional coordinates for protons for example exceeds that of those derived experimentally so far with X-rays, and may even rival that of those determined with neutrons.

4.1.2. Energy due to non-adjacent layers. The r.m.s. value of the calculated energy difference between the 16 analogous EDT and EDT:EDT* stackings is only 13 meV per kaolin formula unit (1 meV per kaolin f.u. $\simeq 0.0955$ kJ mol^{-1}). This number corresponds to the sum of random DFT energy calculation errors for models with a widely different cell and symmetry, and energy contribution of different second-neighbour layers. Accordingly, we can claim here that both the energy calculation error and the energy contribution of second-neighbour layers do not individually exceed 13 meV for the r.m.s. value.

Both claims are important pieces of information. First, the standard uncertainties (s.u.s) of our energy calculation errors are capped at 13 meV for the very different cells and symmetries under consideration here. For example, we can then claim with a high degree of confidence that some transformations between neighbouring kaolin layers with calculated energy differences approaching or exceeding 100 meV are highly unlikely for samples synthesized under ambient pressure and temperature conditions. Second, a statistical numerical value is now attached to the energy associated with second-neighbour interactions between kaolin layers. That value is about half that of the thermal activation energy kT, which is around 25 meV at 300 K. That low value is consistent with the widespread occurrence of stacking disorder that is observed in kaolin samples. The availability of this quantitative result should be useful for the discussion of stacking in similarly layered materials made of hydrogen-bonded inorganic polymeric layers. Lizardites immediately come to mind.

4.1.3. Free energy *versus* enthalpy. The existence of only four natural kaolin polytypes (kaolinite, dickite, HP-dickite and nacrite) among the 36 that we examine here is not easily rationalized. Local conditions of temperature, pressure and the exact chemistry of the fluids may cause stacking energy differences with respect to the results of our zero-temperature, zero-pressure, *in vacuo* energy calculations. Local conditions may then favour one EDT (and its EDT* if it applies) over that of kaolinite which we calculate to be the most stable kaolin polymorph at zero temperature and zero pressure, but not by much relative to dickite (K16*b*, *Cc*, 2), which we calculate to be the polytype with the next-lowest energy. In the perspective of the present work, a number of additional polymorphs could very well exist at ambient pressure according to our calculations. In order of increasing energies as we calculated, they are K16*a* with the space group $P3_1$ and energy 8 meV per f.u. (formula unit), K13*b* (*Cc*, 8), K13*a* ($P3_1$, 12), K11*b* (*Cc*, 14) and K2*a* ($P6_1$, 18). Other stackings such as K18*a* or *b* have energies so high that they are very unlikely to crystallize under ambient conditions.

The existence of nacrite and HP-dickite as the only kaolin polytypes observed beside kaolinite and dickite might be used to question the wisdom of the above energy-based prediction because nacrite and HP-dickite do not appear in the above list of low-energy phases. Their energies are 59 and 112 meV per f.u. higher than that of kaolinite. Many other phases in Tables 2(*a*) and (*b*) have lower energy. The answer is that nacrite and HP-dickite present a combination of sufficiently low energy and small cell volume that makes them the stable phase or a metastable phase over a range of pressures. Dickite was experimentally observed to transform to HP-dickite under pressure (Dera *et al.*, 2003). Similarly, our Fig. 4 (described in detail below) suggests that nacrite could form under pressure and then be returned to ambient conditions as a metastable polytype, whereas HP-dickite transforms reversibly to dickite.

In general, the stable phase of a given material at a given pressure P is that with the lowest enthalpy $U + PV$, where U is the total energy of a given amount of that material and V its volume at that pressure. As the PV term is zero at zero

[1] Supplementary data for this paper are available from the IUCr electronic archives (Reference: LM5012). Services for accessing these data are described at the back of the journal.

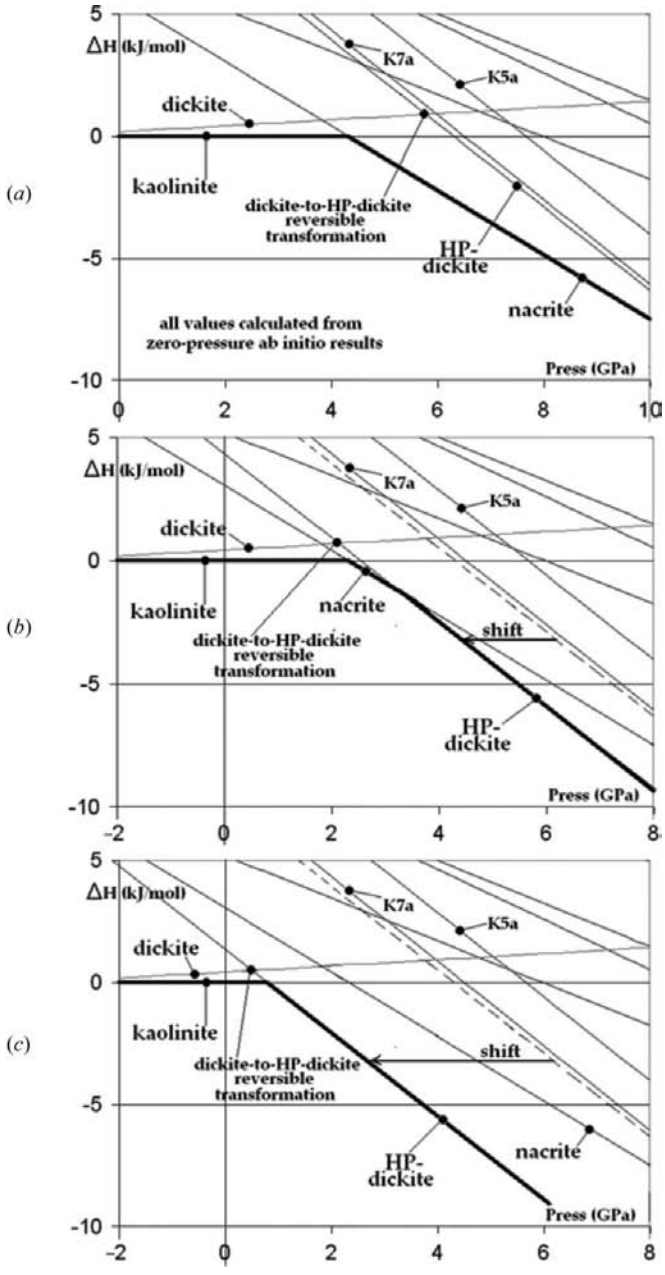

Figure 4
(*a*) Rough enthalpy *versus* pressure graph calculated with $\Delta H = \Delta U + P\Delta V$ for all models with calculated cell volume V per formula unit not larger than that of dickite. Kaolinite and nacrite appear as the successive stable polytypes of kaolin in the bold segments of their enthalpy *versus* pressure line. Dickite transforms reversibly into HP-dickite and not nacrite because transformation to HP-dickite does not involve kaolin-layer rotations, whereas transformation to nacrite would. (*b*) Same as Fig. 4(*a*), but for 300 K, based on two assumptions: first an expected 2 GPa offset for all calculated pressures, and second a speculative shift to the left by ~ 5 MPa K^{-1}, *i.e.* 1.5 GPa at 300 K, of the enthalpy line for HP-dickite. The large 0 K stability domain of nacrite seen in Fig. 4(*a*) is much narrower here and the dickite/HP-dickite transformation occurs at 2 GPa. (*c*) Same as Fig. 4(*b*), but for 600 K. The shift for HP-dickite is then by ~ 3 GPa and nacrite has no stability domain at this temperature. See §4.2.3 for the rationale that (*b*) and (*c*) derived from purely calculated Fig. 4(*a*) using the two assumptions above would explain nearly quantitatively the bulk of current observations about crystallization, diagenesis and transformation of phases in the kaolin system.

pressure, the lowest total energies U that we calculate for models at zero pressure are the lowest enthalpies for phases that are then likely to exist at zero pressure. Dickite and kaolinite are among those. At non-zero but small pressures, the volume per f.u. is not expected to change very differently for the various stackings, but that volume is different for the various models. We call ΔU the energy difference and ΔV the volume difference, both per formula unit between those for a kaolin phase under consideration and those for kaolinite. The enthalpy difference between the given phase and kaolinite is then $\Delta H = \Delta U + P\Delta V$. As can be seen in Table 2, 15 models have lower cell volume per f.u. than kaolinite and are accordingly potential candidates for stable high-pressure kaolin phases. They are: K17 ($\Delta U = +72$ meV per f.u., $\Delta V = -1.450$ Å^3), K5*a* (137, −2.863), K18*a* (183, −1.387), K3*a* (119, −1.081), K7*a* (117, −2.879), K19*a* (107, −1.468), K20 (131, −0.972), K6*b* (78, −0.061), K9*b* (59, −2.179), K18*b* (182, −1.350), K3*b* (106, −0.860), K7*b* (112, −2.843), K10*b* (132, −0.826), K19*b* (112, −1.706) and K5*b* (135, −0.796). After conversion of ΔU to J mol^{-1} and ΔV to m^3 mol^{-1} (P is expressed in Pa), the formula $\Delta H = \Delta U + P\Delta V$ is evaluated for a number of pressures. Those enthalpy numbers are then reported on the graph in Fig. 4(*a*) in units of kJ mol^{-1} for ΔH and GPa for pressures. *Ab initio* values for U and V are both calculated quite precisely, but are known to be affected by a calculation bias that does not vary much with the polytype considered. It follows that calculated values for ΔU and ΔV are then sufficiently accurate for the purpose of the graph in Fig. 4(*a*).

4.1.4. Stability domain of kaolin minerals at 0 K. At face value, the novel overall picture of the stability of the various kaolin polytypes presented in Fig. 4(*a*) appears to be remarkably logical and enlightening. It should nevertheless be interpreted with caution in view of the s.u.s on the free-energy differences and the cell-volume differences that enter in the calculation. According to numbers straight from zero-pressure VASP calculations, the stable phase at zero pressure is kaolinite, but not by much. Dickite is a very close second that might actually be first within the error bar on energies. However, its calculated enthalpy difference with kaolinite increases with pressure, definitely making kaolinite the stable phase and dickite a metastable one under small pressures. At ~ 4 GPa, the phase with lowest enthalpy becomes nacrite. At greater pressures, HP-dickite might become the stable phase, with enthalpy virtually indistinguishable from that of model K7*a* with the space group $P3_1$. However, we feel that this is just a possibility as this conclusion derives from a linear extrapolation over quite a long range. Not too far in enthalpy in the high-pressure range is model K5*a*, with the space group $P1$. We do not claim any accuracy for pressures derived in the above enthalpy calculations (Fig. 4*a*) that aim to qualitatively explain why a higher energy combined with a smaller volume per formula unit might lead to a phase that is stable under pressure. We could have performed the same calculations in a black-box fashion with *VASP*, but we would then have lost the physical sense of why enthalpies evolve that way without ending up with much more authoritative pressures. We are

here at about the current limit of the accuracy for deriving safe conclusions with DFT methods. However, the known mineral phases of kaolin turn out to be calculated here as the low-enthalpy polytypes of kaolin down to considerable pressures in a thorough study of 36 models shown to be possible low-energy models. This is an extremely encouraging result in itself for the usefulness of DFT *ab initio* analyses.

Long linear extrapolations would place the stability of HP-dickite only above 12.5 GPa. This seems to be in contradiction with the fact that it can be produced experimentally by compression of dickite to 2.0 GPa (Dera *et al.*, 2003). This apparent contradiction is not as serious as it sounds because the reversible transformation is from dickite. Our Fig. 4(*a*) places the pressure for dickite $\leftrightarrow$ HP-dickite transformation at around 5.6 GPa, which is tolerably close to the 2 GPa experimental value. We would for example not be surprised by a same pressure offset of ~ 3 GPa in all our pressure calculations. Pressure offsets of this magnitude are commonly corrected for in elasticity *versus* pressure studies. They are due to slight imperfections in the atomic potentials used in all the DFT programs. At pressures greater than 5.6 GPa, we predict HP-dickite to be metastable, but nothing bars its possible existence. Reversible solid-state transformation between dickite and HP-dickite is not surprising because it only involves a shift by $-\mathbf{a}/3$ between adjacent layers that can be obtained from Table 2. Hydrogen bonds can easily shift from one O atom to a neighbouring O atom. This is demonstrated by the existence of plastic deformation, layer slipping or inelastic bending in a number of hydrogen-bonded solids, similar to what happens in solids where the cohesion is due to van der Waals forces. In other words, the transformation is possible because it involves only atomic-level slipping between adjacent layers with no rotation. This concept essentially rules out solid-state transformations between kaolinite, nacrite and dickite because Table 2 shows that all three materials belong to different columns. Solid-state transformation of one into another one would involve rotation of layers with respect to one another. This is not possible. Angular mismatch of layers can happen at crystallization time, but layer rotation is ruled out as a long-range solid-state transformation because it would involve macroscopic atom displacements.

4.1.5. Literature structure for nacrite. We systematically generated calculated powder patterns for the ideal models as a precaution against error or duplication during model generation. To our surprise, those for models K6*b* and K9*b* came out numerically identical. Suspecting a typo in the input or a flaw in our theoretical considerations, we examined closely the two models obtained by $\pi/3$ rotation in both cases followed respectively by translation of $(2\mathbf{a}+\mathbf{b})/3$ and $(\mathbf{a}+2\mathbf{b})/3$, complemented by the enantiomorphic operation [rotation by $5\pi/3$ followed respectively by translation of $(\mathbf{a}+2\mathbf{b})/3$ and $(2\mathbf{a}+\mathbf{b})/3$]. In general, models built on the enantiomorphic pair of rotations R/R^* and translations T/T^* are $[RT{:}R^*T^*]$ and $[RT^*{:}R^*T]$. They are superposable to their respective enantiomorphs, $[R^*T^*{:}RT]$ and $[R^*T{:}RT^*]$, but they are distinguishable from one another. They are accordingly not enantiomorphic and not superposable. This point can be easily verified by calculating the powder patterns for models K7*b* and K10*b*: they are different. Here, models K6*b* and K9*b* are geometrically distinguishable with identical calculated single-crystal and therefore powder diffraction intensities, and are therefore homometric models. The item would remain a theoretical curiosity if model K9*b* did not correspond to that for nacrite, raising the possibility of an incorrect experimentally derived structure. Closer examination of the corresponding quantum-optimized models and comparison with the experimentally determined cell and structure distortions indicated that the latest structure refinement for nacrite (Zheng & Bailey, 1994) clearly displays the specificities of optimized model K9*b* rather than those of optimized model K6*b*. Contrary to model K6*b*, model K9*b* has a stability range in Fig. 4(*a*). The structure results for nacrite, *e.g.* as printed by Zheng & Bailey (1994), are accordingly correct.

4.2. Comparison with literature results

4.2.1. *Ab initio* work. Hyde *et al.* (2002) report that 'zero-pressure kaolinite and dickite are more stable than nacrite, with the difference in zero pressure energy between kaolinite and dickite within the error [bar]'. From blind optimization of ideal models, we find exactly the same thing. We agree with their interpretation of the dickite-to-HP-dickite reversible transformation. We are comfortable with their prediction that a similar, reversible transformation probably exists for kaolinite. The linear extrapolation in Fig. 4(*a*) combined with Table 2 tells us that the transformation might then be with K5*a* at around 7.5 GPa because both K5*a* and K11*a* (= kaolinite) involve no rotations of kaolin layers. In contrast, and contrary to their suggestion, we foresee no similar solid-state reversible phase transformation under pressure for nacrite because entries in our Table 2 that might reach lower enthalpies than nacrite present a different layer-to-layer rotation. Transformation would then involve reconstruction of layers and would accordingly not be reversible.

In a recent first-principles study of OH-stretching modes in kaolinite, dickite and nacrite, Balan *et al.* (2005) report calculated total energies for the three polymorphs to be similar within 1 kJ mol^{-1}, *i.e.* about 10 meV per f.u. We find an energy spread of 59 (13) meV per f.u. for the same quantity. K meshes for total energy calculations are $3 \times 3 \times 3$ in Balan *et al.* and $6 \times 6 \times 6$ here. It follows that Balan's s.u.s on energy could hardly be smaller and are more probably larger than ours. The two sets of reported values are then more or less in statistical agreement in view of the reported or implicit s.u. values.

4.2.2. Experimental measurements of free energy. De Ligny & Navrotsky (1999) performed free-energy measurements on natural samples of kaolinite and dickite. Taking into account the fact that 'error bars' on their measurements are actually twice the s.u. derived from repeated measurements, their reported difference between the free energies of kaolinite and dickite is then -14.3 (4.3) kJ mol^{-1}. This measured

Table 3
Correspondence of reference systems between various authors.

	Axes and origin of			
In terms of	This study	Newnham (1962)	Zvyagin (1962)	Bookin *et al.* (1989)
This study	–	$-\mathbf{a}$, $-\mathbf{b}$, $\mathbf{c}$	$\mathbf{a}+\mathbf{b}$, $\mathbf{a}-\mathbf{b}$, $-\mathbf{c}$	$-\mathbf{a}$, $-\mathbf{a}-2\mathbf{b}$, $\mathbf{c}$
	–	0, 0, z	$-1/3$, $-1/3$, z	0, 0, z
Newnham	$-\mathbf{a}$, $-\mathbf{b}$, $\mathbf{c}$	–	$-\mathbf{a}-\mathbf{b}$, $-\mathbf{a}+\mathbf{b}$, $-\mathbf{c}$	$\mathbf{a}$, $\mathbf{a}+2\mathbf{b}$, $\mathbf{c}$
	0, 0, z	–	1/3, 1/3, z	0, 0, z
Zvyagin	$(\mathbf{a}+\mathbf{b})/2$, $(\mathbf{a}-\mathbf{b})/2$, $-\mathbf{c}$	$(-\mathbf{a}-\mathbf{b})/2$, $(-\mathbf{a}+\mathbf{b})/2$, $-\mathbf{c}$	–	$(-\mathbf{a}-\mathbf{b})/2$, $(-3\mathbf{a}+\mathbf{b})/2$, $-\mathbf{c}$
	1/3, 0, z	1/3, 0, z	–	1/3, 0, z
Bookin	$-\mathbf{a}$, $(\mathbf{a}-\mathbf{b})/2$, $\mathbf{c}$	$\mathbf{a}$, $(-\mathbf{a}+\mathbf{b})/2$, $\mathbf{c}$	$(-\mathbf{a}-\mathbf{b})/2$, $(-3\mathbf{a}+\mathbf{b})/2$, $-\mathbf{c}$	–
	0, 0, z	0, 0, z	1/6, 1/6, z	–

value could be said to be statistically consistent at the 2.5 s.u. level with our calculated value of −0.2 (1.3) kJ mol^{-1} for the same quantity, but this might be somewhat stretching things. In contrast, their enthalpy difference between dickite and nacrite is −3.6 (4.8) kJ mol^{-1}. If we compare here as a first approximation enthalpy differences and free-energy differences, this measured value is in full statistical agreement with our calculated value of −5.5 (1.3) kJ mol^{-1}.

One recent thermochemical study on exceptional samples of dickite (Fialips *et al.*, 2003) revises its free energy to be 18.5 (3.3) kJ mol^{-1} higher than that of kaolinite. Assuming that we would fix the measured value for kaolinite at the value that we calculate, we might then use the experimental value for dickite instead of our calculated value to assemble Fig. 4(*a*). That experimental enthalpy of dickite would then be more than 10 kJ mol^{-1} above the top of the scale on our Fig. 4(*a*), placing it together with our very worst models. This would offer no rationale for its observed existence. We would in particular conclude that HP-dickite could be brought to room pressure and therefore dickite would not exist at all, which is in sharp contradiction with observations. If we instead fix the new experimental energy of dickite at our calculated energy, kaolinite would then be below the limit of the enthalpy scale on Fig. 4(*a*). The appealing stability sequence *versus* pressure that we detail in §4.1 above would be ruined, with no stability domain for anything but kaolinite up to pressures of about 17 GPa. This does not make much sense either. Our interpretation is that something is wrong with all the accepted literature experimental measurements of the free energy of bulk kaolinite. In view of the great care in experiment and analysis involved in the mutually consistent studies by De Ligny & Navrotsky (1999), Fialips *et al.* (2003) as well as others, this is clearly not due to a flawed experiment or to especially impure kaolinite samples. We do not really know, but our preferred hypothesis is that the existence of strongly hydrogen-bonded water on the comparatively large surface area of kaolinite nanocrystals present in all natural samples of kaolinite somehow complicates the weight loss measurement. In contrast, free energies for dickite and nacrite were measured using larger crystals presumably not subject to the above problem. Provided that the free-energy measurements for kaolinite are discarded, our *ab initio* results agree with those for dickite and nacrite within their respective s.u.s.

4.2.3. Diagenetic kaolin minerals. Kaolinite is extremely abundant at the surface of the earth, but dickite is by no means rare, whereas nacrite is quite uncommon. There are many literature reports about occurrences of diagenetic kaolinite and dickite in sandstones (Ruiz Cruz & Moreno Real, 1993; Morad *et al.*, 1994; Parnell *et al.*, 2000; Chen *et al.*, 2001; Lanson *et al.*, 2002; Girard *et al.*, 2002; Patrier *et al.*, 2003; Goemaere, 2004), which sometimes also include the observation of nacrite (Chen *et al.*, 2001; Goemaere, 2004). At face value, this is in sharp contradiction with Fig. 4(*a*) and its discussion in §4.1.4, which tells us that dickite is never the stable phase and should therefore not form, especially not under the moderate pressure (very few GPa) at which it is observed to form by diagenesis.

Modification of Fig. 4(*a*) explaining qualitatively kaolin diagenesis: Fig. 4(*a*) displays $\Delta H(P)$. It is therefore the section at $T = 0$ of $\Delta H(P,T)$ that we denote $\Delta H(P,T = 0)$. Another section at temperature $T_0 \neq 0$, then denoted $\Delta H(P,T = T_0)$ will also be made, not only of straight lines, but those lines will be parallel to the lines in Fig. 4(*a*). This is because the slope of the line $\Delta H = \Delta U + P\Delta V$ is the cell-volume difference ΔV between the polytype considered and that of kaolinite. This volume difference will not vary appreciably with temperature because it depends on the thermal volume expansion of the material, which is expected to be both very tiny and also quite similar from polytype to polytype. Temperature only shifts the lines in Fig. 4(*a*), and probably by not very much. We do not know the amount by which temperature shifts them, but we can speculate by trying to answer the question: Could observations for diagenetic kaolin mineral formation be explained qualitatively using only a slight shift of lines in Fig. 4(*a*)? The answer is yes: we only need to move the line for HP-dickite to the left by about 1.5 GPa, thus intersecting the kaolinite horizontal line barely to the right of where the nacrite line intersects it, as shown in Fig. 4(*b*).

Such a shift would leave a very small pressure-stability range for nacrite, wedged between kaolinite at lower pressures and HP-dickite at higher, but nevertheless moderate pressures. Diagenesis would then happen as follows. No direct transformation of kaolinite into dickite or nacrite occurs at any point of this process. As explained in §4.1.4, this is not a likely solid-state transformation because it would involve reconstruction of kaolin layers. The various phases (kaolinite,

nacrite and HP-dickite) instead crystallize in the pores of the sandstone from dissolved matter according to their respective domain of stability. As shown by Fig. 4(*a*), kaolinite and nacrite can then be brought back to room pressure. HP-dickite instead transforms reversibly into dickite, which is accordingly the phase observed in the laboratory, whereas the phase that crystallized was HP-dickite. This is consistent with the following observations. Sandstones containing diagenetic kaolin minerals only contain kaolinite if they were exposed to only moderate pressures (~ 1 GPa or less) and accordingly moderate temperatures. Those that were exposed to greater pressures (~ 2 GPa or more), and accordingly higher temperatures, often contain a mixture of well crystallized kaolinite and well crystallized dickite, but some of them contain only dickite. We interpret the different crystals as produced by crystallization at different depths, either during descent or ascent, but with no later transformation of one into the other. The unusual samples that are reported to contain nacrite seem to always also contain both kaolinite and dickite. We interpret this as being due to the narrow range of stability of nacrite, wedged in-between that of kaolinite at lower pressures and that of HP-dickite at higher pressures.

Speculative modification that would explain quantitatively most observations: Actually, the pair of graphs shown in Figs. 4(*b*) [$\Delta H(P,T \simeq 300$ K)] and (*c*) [$\Delta H(P,T \simeq 600$ K)] would explain quantitatively nearly all the observations that we know of about the system of kaolin minerals. Graphs in Figs. 4(*b*) and (*c*) derive from the $T = 0$ K diagram calculated in Fig. 4(*a*) by two assumptions. The first one is a correction for a 2 GPa bias in calculated pressures. The sense and magnitude for that bias are those expected from our long practice of elastic tensor calculations, which involves a wealth of experimental data to compare with. As explained in §4.1.4, we would not have been surprised by an even greater pressure bias. The second assumption would be a temperature-dependent shift to the left by about 5 MPa K^{-1} for the line about HP-dickite. That assumption is mostly speculative, but it is tempting to consider the concept because the whole puzzle of the kaolin system would then fall into place almost quantitatively, as detailed below. The assumption is supported somewhat by widespread remarks, *e.g.* in Parnell *et al.* (2000), to the effect that dickite is an indicator of higher temperatures.

In Fig. 4(*b*), we then read that only kaolinite forms under ambient pressure and temperature conditions, as is observed. Dickite is metastable at all pressures and temperatures. Its observed existence at room temperature and pressure results from the crystallization of HP-dickite and its reversible transformation into dickite. This graph also places the reversible dickite–HP-dickite transformation at ~ 2 GPa at room temperature, as observed by Dera *et al.* (2003). Under a normal geothermal gradient, HP-dickite would start forming above 1 GPa for temperatures around 500 K, and come back to room conditions as dickite, as is observed. The stability domain for nacrite would be a narrow triangle in projection on the *PT* plane of $H(P,T)$. The domain in which nacrite would form, which is narrow at room temperature, would taper off at about 400–450 K. Crystallization of nacrite would then require a combination of depth and temperature that is not really likely for a normal geothermal gradient. It is accordingly a rare diagenetic mineral, mostly observed in veins, always in association with both kaolinite and dickite. Reports implying the mutual transformation of kaolinite, dickite or nacrite into one another clearly involve dissolution and recrystallization, and not solid-state transformation, in agreement with views developed here.

4.2.4. Stacking disorder observed in natural kaolinite. Stacking disorder in kaolinite samples has been the subject of numerous sophisticated powder-diffraction studies for half a century. The real-space interpretation of the result of those experiments has evolved over time and may not be final. Reasonings in §3.4.2 here support an analysis in Bookin *et al.* (1989) that explains how the '**b**/3 step faults' (in their reference system) observed in kaolinite are consistent with faults owing to the existence of enantiomorphic kaolinite transformations between adjacent layers. Restated from the viewpoint of the present study, real kaolinite crystals would mostly be made of the same EDT stacking, but with its EDT* as the prevalent stacking fault. This makes a lot of sense in view of the argument for creating low-energy polytypes presented in §3.4.2. This causes the faulted single crystal to display occasional shifts of the Al vacancy pattern by a third of the long diagonal of our pseudo-hexagonal (**ab**) mesh, *i.e.* our $[\bar{1}10]$ direction. Diffuse diffraction features caused by stacking steps along this direction are hardly distinguishable by powder work from features occurring along our [120] direction because the (**ab**) mesh is metrically quasi-hexagonal. This [120] direction is Bookin's $-$**b** direction. In other words, Bookin's explanations for the main stacking disorder experimentally observed in kaolinite are consistent with the energy-based views presented in §3.4.2 of the present work. The tiny energy difference that we calculate between kaolinite and dickite stackings also allow the existence of dickite faults in kaolinite. This would involve either pure $4\pi/3$ rotations of layers with respect to the **a**/3 layer-to-layer translation implicit in the kaolinite stacking or $2\pi/3$ rotations combined with (**b** $-$ **a**)/3 steps (our reference system), *i.e.* again Bookin's '**b**/3 steps' combined with $2\pi/3$ rotations for right-handed kaolinite.

4.2.5. Distances between cations in neighbouring layers. Newnham (1962) analyzes the Si/Al cation–cation approaches from different layers as well as OH$\cdots$O approaches, giving semi-quantitative negative scores to short interlayer Si$-$Si, Si$-$Al, Al$-$Al distances as well as long OH$\cdots$O oxygen–oxygen approaches. It is a fact that the two kaolin polytypes known in 1962, kaolinite and dickite accumulate small scores in his tabulation. If we compare Newnham's scores with our calculated energies for the various transformations in Table 2, stackings with the highest energies receive large negative scores, whereas those with the lowest energies mostly receive small scores. However, stackings in the mid-range of energies can just as well receive very large or very small scores. In other words, Newnham's criterion is one aspect of a more complex picture.

4.2.6. Correspondence between reference systems used. Several reference systems have been used by various authors.

Some of them are explicitly defined, whereas others are only implicit, either from references or from drawings. Table 3 prints the transformations of axes and origin between the various authors or groups of authors as a help for readers.

5. Conclusions

We have clearly split the well known 36 geometrically distinguishable stackings of two kaolinite layers into 20 energy-distinguishable stackings and 16 enantiomorphic ones. The assumption that interactions between non-adjacent kaolin layers constitutes a tiny correction to interactions between adjacent layers implies that the architectures of lowest-energy kaolin polytypes most probably result from one of the two following mechanisms. Mechanism (*a*) is the repeated application of the same stacking of two layers. Mechanism (*b*) is the alternate application of a two-layer transformation followed by that of the enantiomorphic transformation. Analysis of the results from blind *ab initio* optimization of the 36 resulting energy-distinguishable crystalline stackings built from an undistorted ideal kaolin layer produced numerous results and conclusions, among which are the following:

(i) All four currently known crystalline polytypes of kaolin (kaolinite, dickite, nacrite and HP-dickite) are among the 36 optimized models, displaying approximately the same cell and polyhedral distortions as the experimental results, in support of the above assumption and of the modeling abilities of DFT methods.

(ii) Optimized hydrogen positions are included with all 36 deposited optimized models. This constitutes important new results, even for the four known polytypes.

(iii) Kaolinite and dickite, the most frequently observed kaolin minerals, are the lowest-energy solutions at zero pressure. A number of never-observed other optimized models definitely have calculated total energies higher than that of kaolinite, but lower than those for nacrite and HP-dickite.

(iv) From straightforward calculations on *ab initio* zero-pressure total energies and cell volumes, we present a semi-quantitative phase diagram of stable kaolin polytypes *versus* moderate pressure in Fig. 4(*a*). Kaolinite, then nacrite and then possibly HP-dickite are the low-enthalpy phases and therefore the likely stable kaolin phases up to considerable pressures.

(v) At face value the numerical results indicate that dickite is metastable at all pressures, but with a total energy that is practically indistinguishable from that of kaolinite at zero pressure. Its transformation to HP-dickite is predicted here to happen around 5.6 GPa, a value that is not inconsistent with the observed 2.0 GPa in view of the gross approximations involved. The reason for a solid-state transformation from metastable dickite to metastable HP-dickite rather than nacrite that is stable at that pressure is explained.

(vi) Synthesis might be possible, but only at ambient pressure, for a short list of kaolin polytypes that we state. If these polytypes were obtained in a synthesis, successful structure solution could presumably require only cell and symmetry comparisons with entries in our deposited Table S1, followed by structure-factor calculations using the experimental cell and the *ab initio* fractional coordinates.

(vii) Two modifications of the purely calculated Fig. 4(*a*), namely a correction for an expected calculated pressure bias of 2 GPa and a speculative shift by ~ 5 MPa K^{-1} of the isothermal enthalpy line for HP-dickite, are presented in Figs. 4(*b*) and (*c*). They would explain nearly quantitatively the bulk of current observations about the kaolin system.

(viii) The ideal model for nacrite is shown to be homometric with another ideal model in the series. The crystal structure for nacrite in the literature is shown to be that of the stable member of that pair, and is therefore correct.

(ix) Our energy considerations and results are consistent with stacking defects observed in natural kaolinite, as analyzed by Bookin *et al.* (1989).

(x) The r.m.s. value of random errors on the total energy differences calculated *ab initio* does not exceed 13 meV per f.u. here.

(xi) The r.m.s. contribution of non-adjacent kaolin-layer interactions to total energy does not exceed 13 meV per f.u.

(xii) In our opinion, all the recent literature measurements of the Gibbs free-energy difference between kaolinite and dickite, and especially the authoritative -18.5 (3.3) kJ mol^{-1} measured by Fialips *et al.* (2003), do not correspond to that between bulk dickite and bulk kaolinite materials.

The above conclusions and observations entirely derive from numbers obtained *ab initio*. They may have to be interpreted with caution in view of the uncertainties on total energies and cell volumes. Nevertheless, in view of the rationality of the novel overall picture of the kaolin system that emerges from our calculations here, we trust that the above conclusions are globally sound. They are not the final picture, but they certainly point in the right direction and constitute a guide for future experiments, calculations and interpretations. In particular, our deposited Table S1 contains a wealth of untapped structural information. It can for example become the starting point for an accurate enthalpy *versus* pressure study that would clarify our Fig. 4 by avoiding the simplifications in the present contribution, and thus place it on a fully quantitative basis. We nevertheless feel that the present *ab initio* study has opened a surprising number of new perspectives for thought and avenues for research in an otherwise rather well studied but difficult system of great practical importance.

Ab initio studies of the magnitude of the present one, involving numerous accurate optimizations of models with up to 102 atoms per primitive cell over a whole crystal-chemical system, here the kaolin minerals, have become possible only recently. This is due both to the magnitude of the modeling challenge and to the computing costs involved. We accordingly hope that the present study might become a prototype for new types of theoretical contributions aiming at clarifying concepts about whole crystal-chemical systems, thus constituting a source of inspiration for future experimental developments. In the present work, the systematic theoretical study of kaolin polytypes was made possible through modeling, as well as quantum input preparation and interpretation with *Materials*

Toolkit (Le Page & Rodgers, 2005) together with quantum optimizations performed with *VASP* (Kresse, 1993; Kresse & Hafner, 1993).

This work was supported in part through the Climate Change Technology and Innovation program of the Canadian government. We thank both anonymous referees for detailed reviews, especially Referee 1 for the suggestion to add a discussion about the diagenesis of kaolin minerals.

References

Adams, J. M. (1979). *Acta Cryst.* B**35**, 1084–1088.
Adams, J. M. (1983). *Clays Clay Miner.* **31**, 352–356.
Adams, J. M. & Jefferson, D. A. (1976). *Acta Cryst.* B**32**, 1180–1183.
Bailey, S. W. (1963). *Am. Miner.* **48**, 1196–1209.
Bailey, S. W. (1988). *Mineral. Soc. Am. Rev. Miner.* **19**, 675–725.
Bailey, S. W. & Banfield, J. F. (1995). *Am. Mineral.* **80**, 1104–1115.
Balan, E., Lazzeri, M., Saitta, A. M., Allard, T., Fuchs, Y. & Mauri, F. (2005). *Am. Mineral.* **90**, 50–60.
Banfield, J. F. & Bailey, S. W. (1996). *Am. Mineral.* **81**, 79–91.
Banfield, J. F., Bailey, S. W., Barker, W. W. & Smith II, R. C. (1995). *Am. Mineral.* **80**, 1116–1131.
Bish, D. L. (1993). *Clays Clay Miner.* **41**, 738–744.
Bish, D. L. & Johnston, C. T. (1993). *Clays Clay Miner.* **41**, 297–304.
Bish, D. L. & Von Dreele, R. B. (1989). *Clays Clay Miner.* **37**, 289–296.
Blount, A. M., Threadgold, I. M. & Bailey, S. W. (1969). *Clays Clay Miner.* **17**, 185–194.
Bookin, A. S., Drits, V. A., Plançon, A. & Tchoubar, C. (1989). *Clays Clay Miner.* **37**, 297–307.
Chen, P. Y., Wang, M. K. & Yang, D. S. (2001). *Clays Clay Miner.* **49**, 586–595.
Davidson, E. R. (1983). *Methods in Computational Molecular Physics*, edited by G. H. F. Diercksen & S. Wilson, Vol. 113, Ser. C, p. 95. New York: NATO Advanced Study Institute, Plenum Press.
De Ligny, D. & Navrotsky, A. (1999). *Am. Mineral.* **84**, 506–516.
Dera, P., Prewitt, C. T., Japel, S., Bish, D. L. & Johnston, C. T. (2003). *Am. Mineral.* **88**, 1429–1435.
Dornberger-Schiff, K. & Durovič, S. (1975*a*). *Clays Clay Miner.* **23**, 219–229.
Dornberger-Schiff, K. & Durovič, S. (1975*b*). *Clays Clay Miner.* **23**, 231–246.
Drits, V. A. & Kashaev, A. A. (1960). *Sov. Phys. Crystallogr.* **5**, 207–210.
Durovič, S., Miklos, D. & Dornberger-Schiff, K. (1981). *Cryst. Res. Technol.* **16**, 557–565.
El-Sayed, K., Keiba, S. K. & Abdel-Rahman, A. M. (1990). *Cryst. Res. Tecnol.* **25**, 305–312.
Fialips, C. I., Majzlan, J., Beaufort, D. & Navrotsky, A. (2003). *Am. Mineral.* **88**, 837–845.
Giese, R. F. Jr (1988). *Mineral. Soc. Am. Rev. Miner.* **19**, 29–66.
Girard, J.-P., Munz, I. A., Johansen, H., Lacharpagne, J.-C. & Sommer, F. (2002). *J. Sediment. Res.* **72**, 746–759.
Goemaere, E. (2004). *Geol. Belg.* **7**, 285–311.
Gregorkiewitz, M., Lebech, B., Mellini, M. & Viti, C. (1996). *Am. Mineral.* **81**, 1111–1116.
Hyde, R. A., Steinle-Neumann, G. & Dera, P. (2002). American Geophysical Union, Fall Meeting 2002, Abstr. #T21C-1109.
Joswig, W. & Drits, V. A. (1986). *Neues Jahrb. Miner. Monatsh.* **1**, 19–22.
Kresse, G. (1993). PhD thesis. Technische Universität Wien, Austria.
Kresse, G. & Hafner, J. (1993). *Phys. Rev. B*, **48**, 13115–13118.
Kresse, G. & Hafner, J. (1994). *Phys. Rev. B*, **49**, 14251–14269.
Kresse, G. & Joubert, J. (1999). *Phys. Rev. B*, **59**, 1758–1775.
Lanson, B., Beaufort, D., Berger, G., Bauer, A., Cassagnabere, A. & Meunier, A. (2002). *Clay Miner.* **37**, 1–22.
Le Page, Y. & Rodgers, J. R. (2005). *J. Appl. Cryst.* **38**, 697–705.
Mercier, P. H. J., Le Page, Y., Whitfield, P. S., Mitchell, L. D., Davidson, I. J. & White, T. J. (2005). *Acta Cryst.* B**61**, 635–655.
Methfessel, M. & Paxton, A. T. (1989). *Phys. Rev. B*, **40**, 3616–3621.
Monkhorst, H. J. & Pack, J. D. (1976). *Phys. Rev. B*, **13**, 5188–5192.
Morad, S., Ben Ismail, H. N., De Ros, L. F., Al-Aasm, I. S. & Serrhini, N.-E. (1994). *Sedimentology*, **41**, 1253–1272.
Murray, H. H. (1991). *Reviews in Mineralogy*, Vol. 19, edited by S. W. Bailey, pp. 67–89. Washington, DC: Mineralogical Society of America.
Neder, R. G., Burghammer, M., Grasl, T. H., Schulz, H., Bram, A. & Fiedler, S. (1999). *Clays Clay Miner.* **47**, 487–494.
Newnham, R. E. (1962). *Mineral. Mag.* **32**, 683–704.
Parnell, J., Baron, M. & Boyce, A. (2000). *J. Geol. Soc. (London)*, **157**, 635–640.
Patrier, P., Beaufort, D., Laverret, E. & Bruneton, P. (2003). *Clays Clay Miner.* **51**, 102–116.
Pauling, L. (1960). *The Nature of the Chemical Bond.* New York: Cornell University Press.
Ruiz Cruz, M. D. & Moreno Real, L. (1993). *Clays Clay Miner.* **41**, 570–579.
Smrčok, L., Gyepesová, D. & Chmielová, M. (1990). *Cryst. Res. Technol.* **25**, 105–110.
Suitch, P. R. & Young, R. A. (1983). *Clays Clay Miner.* **31**, 357–366.
Toraya, H., Iwai, S. I. & Marumo, F. (1980). *Mineral. J*, **10**, 168–180.
Young, R. A. & Hewat, A. W. (1988). *Clays Clay Miner.* **36**, 225–232.
Zheng, H. & Bailey, S. W. (1994). *Clays Clay Miner.* **42**, 46–52.
Zvyagin, B. B. (1960). *Sov. Phys. Cryst.* **5**, 32–42.
Zvyagin, B. B. (1962). *Sov. Phys. Cryst.* **7**, 36–51.
Zvyagin, B. B., Soboleva, S. V. & Fedotov, A. F. (1972). *Sov. Phys. Crystallogr.* **17**, 44–52.